crystals

MDPI

Article

An Environmentally Stable Organic–Inorganic Hybrid Perovskite Containing Py Cation with Low Trap-State Density

Alex Fan Xu, Ryan Taoran Wang, Lory Wenjuan Yang, Elton Enchong Liu and Gu Xu *

Department of Materials Science and Engineering, McMaster University, 1280 Main Street West, Hamilton, ON L8S 4L8, Canada; xuf21@mcmaster.ca (A.F.X.); wangt41@mcmaster.ca (R.T.W.); yangw48@mcmaster.ca (L.W.Y.); liue26@mcmaster.ca (E.E.L.)

* Correspondence: xugu@mcmaster.ca

Received: 4 March 2020; Accepted: 1 April 2020; Published: 2 April 2020

Abstract: The commonly-employed methylammonium-based perovskites are environmentally unstable, which limits their commercialization. To resolve this problem, a stable hybrid perovskite, pyrrolidinium lead iodide ($PyPbI_3$), was synthesized successfully via a simple drop casting method. The formed $PyPbI_3$ exhibited a hexagonal structure. It presented not only excellent phase stability, but also low trap-state density, as confirmed via the X-ray diffraction and space-charge-limited currents measurements. This novel perovskite may be applicable to perovskite photovoltaics to improve their environmental stability.

Keywords: pyrrolidinium lead iodide; organic–inorganic hybrid perovskite; environmental stability; low trap-state density; phase stability; perovskite solar cell

1. Introduction

With the growing demands for renewable energy, photovoltaics (PV) becomes a popular research area [1,2]. Among all PV materials, organic–inorganic hybrid perovskite (OIHP) has attracted much interest in recent years. In general, OIHP has a formula of ABX_3, where A represents monovalent cations, B for metals (e.g., Pb) and X for halides. Methylammonium lead iodide, with a chemical formula of $MAPbI_3$, has been considered one of the most important OIHP materials [3]. It has been studied and reported that $MAPbI_3$ has many superior properties including long diffusion length [4,5], tunable bandgap [6,7] and high defect tolerance [8], which results in the rapid development of its power conversion efficiency (PCE) from 3.8% to 25.2% [9] within only ten years, making OIHP one of the most promising PV materials.

Despite their excellent performance in terms of energy efficiency, the lifetime of the fabricated perovskite solar cell (PSC) is far from ideal [10]. For example, an unencapsulated PSC device would lose 10%–30% of its initial PCE within only several days in ambient conditions [11]. Comparing that with other already commercialized PV materials such as silicon, which has a lifetime of more than 25 years [12], the much shorter lifetime of PSCs confines them as a lab-scale product.

In order to fight against the $MAPbI_3$ instability problems, numerous methods have been attempted. Although strategies such as interface engineering [13–15] and doping [7,16,17] were shown to improve the environmental stability of $MAPbI_3$ effectively, they did not enhance the lifetime to any appreciable level, as $MAPbI_3$ is intrinsically unstable [10,18].

In this regard, replacing the unstable MA cations seems inevitable. In 2014, formamidinium lead iodide ($FAPbI_3$) [19] was introduced to improve the stability of PSC, but despite the enhanced thermal stability, they suffered severe moisture and phase instability issues [20]. Incorporating small

inorganic cations such as cesium (Cs) to form the perovskite structure was also reported in 2015 [21], and the formed $CsPbI_3$ exhibited improved moisture and thermal stabilities, yet its phase was not stable at room temperature [22]. Most recently, ring-based molecules with a strong hydrophobic nature were considered as an alternative in replacing the conventional unstable MA molecule. In 2017 [23], a four-membered ring-based azetidine (Az) molecule was introduced into the perovskite crystal structure to form $AzPbI_3$. According to the results, the $AzPbI_3$ exhibited excellent moisture stability. However, the structure of $AzPbI_3$ was highly distorted, and its bandgap was not ideal (~2.15 eV). Chao et al. (2018) [24] simulated a three-membered ring-based perovskite, namely aziridinium lead iodide ($AzPbI_3$). Their results indicated that such perovskite exhibited a low bandgap of 1.49 eV, as well as enhanced structural stability compared with $MAPbI_3$ and $FAPbI_3$ in terms of the formation enthalpy. A major issue for $AzrPbI_3$ was that the aziridine molecule was highly toxic, which made it not practical for application. We thus reported in our previous work [25] a five-membered ring-based pyrrolidine (Py) molecule could be used to form a new perovskite pyrrolidinium lead iodide ($PyPbI_3$). The $PyPbI_3$ not only exhibited a lower bandgap (~1.80 eV) than $AzPbI_3$, but also showed good water- and high-temperature-resistance [9], providing a possible answer to the long-term PSC instability problem. However, the phase stability of $PyPbI_3$, equally important to the moisture and thermal stability, remains unknown. Moreover, other properties such as defect states, which affect the perovskite PV performance significantly, also need further investigation.

It is, therefore, the purpose of the current report to investigate the phase stability of $PyPbI_3$. The results of our stability measurements showed that $PyPbI_3$ exhibited only one phase in an ambient environment, indicating its excellent phase stability. The optical properties and morphology of the $PyPbI_3$ film were also evaluated. By conducting the space-charge-limited currents (SCLC) measurement in a capacitor-like device, we revealed that $PyPbI_3$ demonstrated a low trap-state density of ~2.3×10^{16} cm^{-3}, which is comparable to that of $MAPbI_3$. Our results indicated that $PyPbI_3$ is an environmentally stable OIHP material with great potential to be employed in perovskite PV applications.

2. Materials and Methods

2.1. Materials

N,*N*-Dimethylformamide (DMF, 99.99%) and PbI_2 (99.999%) were purchased from Sigma-Aldrich. Pyrrolidine hydroiodide (PyI, 98%) was purchased from TCI America.

2.2. Film Formation and Device Fabrication

The film was fabricated via a simple drop casting method. First, the ITO substrate was sequentially washed with distilled water and ethanol, two times with each. After 20 min of UV–O_3 treatments, 80 µL of PyI (80 mg) and PbI_2 (60 mg) in a DMF solution were drop cast on the substrate. The fabricated films were next annealed on a hot plate at 120 °C for 30 min in air. In the capacitor-like device, the metal electrode was further deposited by thermal evaporation of gold under a pressure of 5×10^{-5} Pa.

2.3. Characterizations

Powder XRD measurements were conducted on a Bruker D8 DISCOVER diffractometer (Bruker Corporation, Billerica, Massachusetts, USA). The steady state photoluminescence (PL) measurement was taken at room temperature with an excitation wavelength of 514.5 nm. The film morphology image was taken by a FEI Magellan 400 XHRSEM scanning electron microscope (SEM) (FEI Company Magellan™ XHR, Midland, ON, Canada). The current density–voltage characteristics of the devices were obtained using a Keithley 2400 source-measure unit. The light intensity was calibrated using a KG-5 Si diode.

3. Results

3.1. Fabrication and Characterizations of the Perovskite Film

The $PyPbI_3$ film was fabricated by employing a simple drop casting method as illustrated in Figure 1 (Details shown in experimental section), following the methods reported in our previous work [9]. The thickness of the formed film was measured as 1500 nm by a profilometer. To investigate the crystal structure of the film, we conducted powder XRD measurements. The results are shown in Figure 2, and suggest the formation of $PyPbI_3$ in the film [9]. The relatively low intensity of the first peak could be attributed to the texture in the powder film.

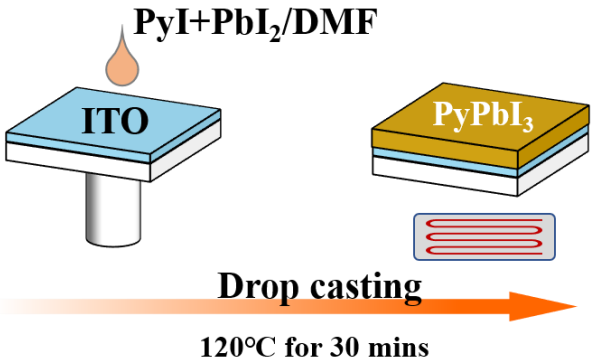

Figure 1. The schematic illustration of the $PyPbI_3$ film fabrication process.

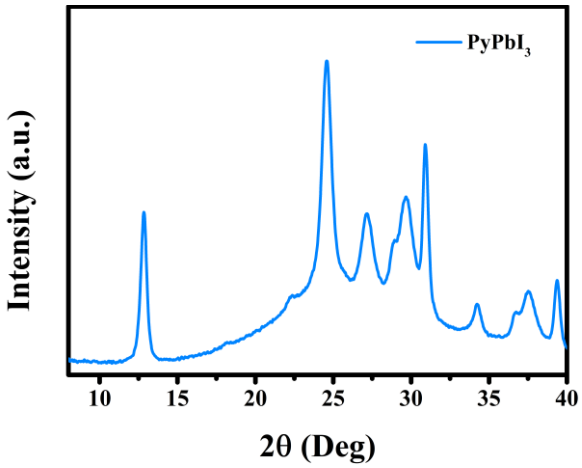

Figure 2. XRD results of the fabricated $PyPbI_3$ film.

The optical property of the $PyPbI_3$ film was evaluated via steady state photoluminescence (PL) measurement. The excitation wavelength adopted in this study was 514.5 nm. The PL result is shown in Figure 3, which shows a peak at around 600 nm, exhibiting a blue shift compared to our previous results [25]. This could be attributed to the different thickness of the perovskite film (in this work 1500 nm), leading to a change of its absorption property, as reported in the literature [26–28]. The relatively broad emission characteristic of the peak further indicates that the structure type of $PyPbI_3$ belongs to 1D perovskite [29]. In addition, the PL luminescence of $PyPbI_3$ remained the same after one hour in ambient conditions, which indicated its good moisture stability.

The morphology of the film was studied via field emission scanning electron microscope (SEM). As shown in Figure 4, the film consisted of many grains of micrometer sizes and had low grain boundary coverage area, which is comparable with that of $MAPbI_3$ [30].

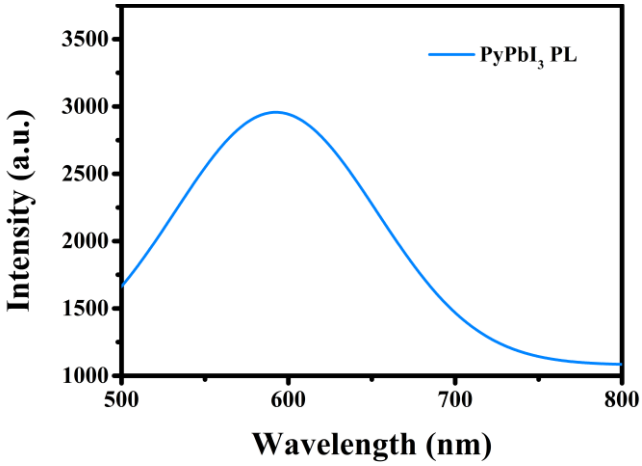

Figure 3. Steady state PL curve of $PyPbI_3$.

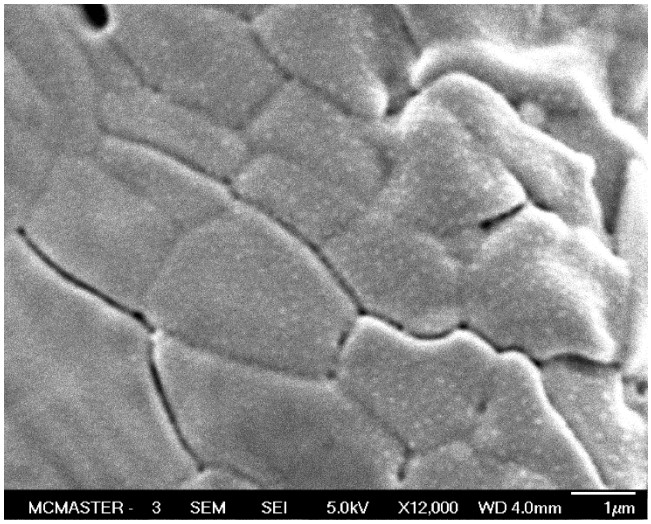

Figure 4. Planar SEM image of $PyPbI_3$.

3.2. Trap-State Density of the $PyPbI_3$ Film

To investigate the defect states in $PyPbI_3$ film, SCLC measurements were taken. We fabricated capacitor-like devices following steps shown in the experimental section. The structure of the device is illustrated in Figure 5, and was composed of ITO/$PyPbI_3$/Au. From the current density–voltage (CV) curve shown in Figure 6, it can be observed that the CV response is ohmic at low voltage. Upon reaching the intermediate voltage, the defect states are filled by the injected charge carriers (refers to TFL), resulting in a linear relationship between the voltage (V_{TFL}) and the density of defect states (N_{DEF}). Following the methods mentioned in previous reports ($N_{DEF} = 2\ \varepsilon\varepsilon_0 V_{TFL}/eL^2$) [11], ε_0 is the vacuum permittivity, ε (~4.90, determined by RUFUTO 871) is the dielectric constant of $PyPbI_3$, L (~1500 nm) is the thickness of the perovskite film, and e is the elementary charge. The defect density was estimated to be 2.3×10^{16} cm^{-3}, which is comparable to that of $MAPbI_3$ (~10^{16} cm^{-3}), indicating a low trap-state density in the polycrystalline film of $PyPbI_3$. The origin of the trap-states in $PyPbI_3$ was assumed to be located at the grain boundaries, as suggested in the literature [31].

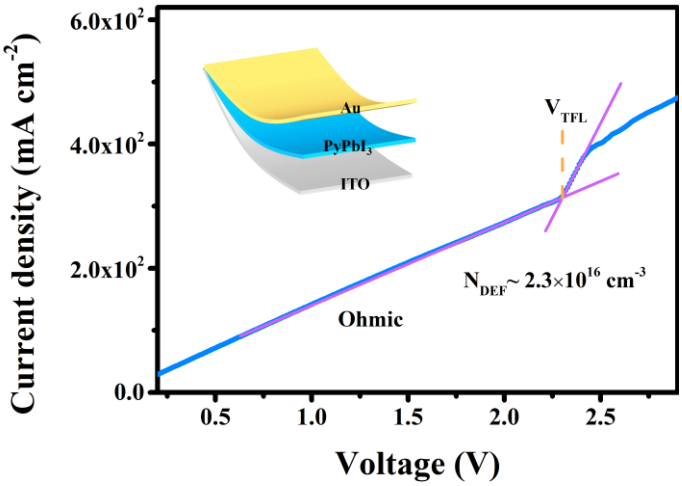

Figure 5. Current–voltage curves of the devices adopting the as-illustrated configuration. Inset: Device scheme of ITO/perovskite/Au.

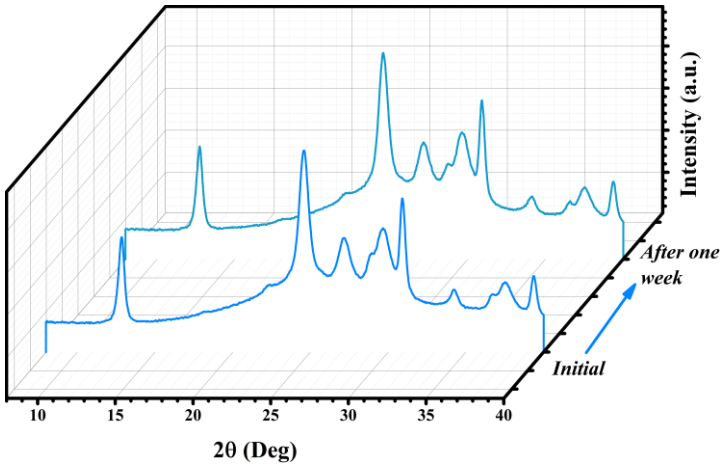

Figure 6. Initial XRD results of $PyPbI_3$, and results after one week in ambient conditions with a RH of 50%.

3.3. Stability Measurements of the $PyPbI_3$ Film

To investigate the phase stability of $PyPbI_3$, a set of stability measurements was conducted. According to previous reports on $MAPbI_3$ and $CsPbI_3$, the perovskite phase transition was triggered by either raising humidity [18,32] or temperature [22]. We therefore conducted the phase stability measurements in two different environments. First, we evaluated the phase stability of $PyPbI_3$ in moisture with a relative humidity (RH) of ~50%. The formed film was kept in a desiccator for one week. The results are illustrated in Figure 7. As can be observed, after one week in an ambient environment, the XRD patterns of $PyPbI_3$ remained unchanged, indicating the moisture and phase stabilities of $PyPbI_3$.

Next, we raised the temperature of the environment. The fabricated film was placed on a hot plate at a temperature of 85 °C for 6 h. From the XRD results (Figure 8), a tiny peak appeared at around 14.78°, correspond to the PbI_2 peak. The PbI_2 peak was assumed to be originated from the surface of the $PyPbI_3$ film, as suggested in literature [33]. Apart from that, we did not observe any other unknow diffraction peak. In addition, previous TGA measurements [9] further indicated the thermal stability of $PyPbI_3$, which is consistent with our XRD results.

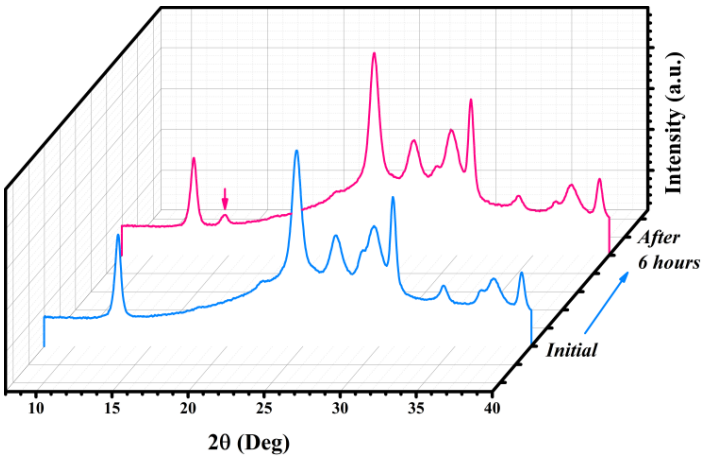

Figure 7. XRD results of $PyPbI_3$ initial and after 6 h with T = 85 °C.

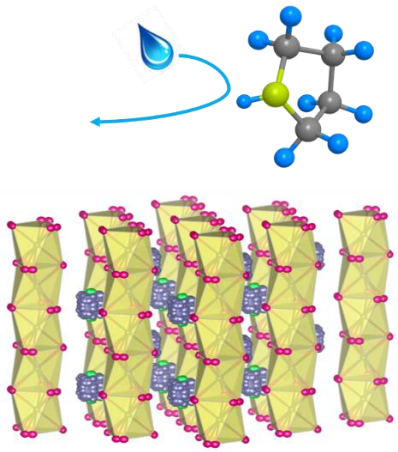

Figure 8. Schematic illustration of water-repelling mechanism in $PyPbI_3$. The top five-membered ring stands for the Py molecule, and structure beneath represents $PyPbI_3$ perovskite.

4. Discussion

The above stability measurement results indicate that $PyPbI_3$ is highly phase-stable. Combining it with previous results, we can therefore conclude that $PyPbI_3$ exhibits excellent environmental stability compared to $MAPbI_3$. The results are further summarized in Table 1. We also explored the reasons for the enhanced environmental stabilities found in $PyPbI_3$. The excellent moisture resistance of the perovskite can be attributed to the strong hydrophobic nature of its pyrrolidine rings [9], which can repel the invasion of water molecules, as schemed in Figure 8. The high thermal stability can be related to the greater molecular weight of the Py molecules (71 g/mol) compared to the MA molecules (31 g/mol), as the former molecule is less volatile [11].

Table 1. Comparison of five OIHPs comparing moisture, thermal and phase stabilities.

Formula	$MAPbI_3$	$FAPbI_3$	$CsPbI_3$	$AzPbI_3$	$PyPbI_3$
Moisture stability	Bad [18]	Bad [31]	Regular [21]	Good [23]	Good [25]
Thermal stability	Bad [34]	Regular [19]	Regular [35]	N/A	Good [9]

5. Conclusions

In conclusion, a five-membered ring-based perovskite $PyPbI_3$ was synthesized and its properties were characterized. The trap-state density of the polycrystalline $PyPbI_3$ film was calculated to be 2.3×10^{16} cm^{-3}. The stability measurements reveal that $PyPbI_3$ is an environmentally stable perovskite,

which shows great potential for employment in PSCs to resolve their long-term instability problems. In the future, it will be of great significance to fabricate and investigate the $PyPbI_3$-only solar cell device.

Author Contributions: Conceptualization, methodology, investigation, writing—original draft preparation, A.F.X.; writing—review and editing, R.T.W. & L.W.Y. & E.E.L.; supervision, project administration, G.X.; All authors have read and agreed to the published version of the manuscript.

Funding: This research was funded by the Natural Science and Engineering Research Council of Canada, grant number 105-46964.

Acknowledgments: The authors would like to acknowledge the experimental supports from the MAX Diffraction Facility from Department of Chemistry, Department of Engineering Physics of McMaster University; Beijing University of Technology; Experimental Centre of Advanced Materials (ECAM) and School of Materials Science and Engineering of Beijing Institute of Technology; Canadian Center for Electron Microscopy (CCEM).

Conflicts of Interest: The authors declare no conflict of interest.

References

1. Rong, Y.; Hu, Y.; Mei, A.; Tan, H.; Saidaminov, M.I.; Seok, S.I.; McGehee, M.D.; Sargent, E.H.; Han, H. Challenges for commercializing perovskite solar cells. *Science* **2018**, *361*, eaat8235. [CrossRef] [PubMed]
2. Li, Z.; Zhao, Y.; Wang, X.; Sun, Y.; Zhao, Z.; Li, Y.; Zhou, H.; Chen, Q. Cost Analysis of Perovskite Tandem Photovoltaics. *Joule* **2018**, *2*, 1559–1572. [CrossRef]
3. Yin, W.J.; Shi, T.; Yan, Y. Unique properties of halide perovskites as possible origins of the superior solar cell performance. *Adv. Mater.* **2014**, *26*, 4653–4658. [CrossRef] [PubMed]
4. Xing, G.; Mathews, N.; Sun, S.; Lim, S.S.; Lam, Y.M.; Grätzel, M.; Mhaisalkar, S.; Sum, T.C. Long-range balanced electron-and hole-transport lengths in organic-inorganic $CH_3NH_3PbI_3$. *Science* **2013**, *342*, 344–347. [CrossRef]
5. Dong, Q.; Fang, Y.; Shao, Y.; Mulligan, P.; Qiu, J.; Cao, L.; Huang, J. Electron-hole diffusion lengths > 175 μm in solution-grown $CH_3NH_3PbI_3$ single crystals. *Science* **2015**, *347*, 967–970. [CrossRef]
6. Wang, R.T.; Xu, A.F.; Yang, W.; Chen, J.Y.; Kitai, A.; Xu, G. Magnetic-field-induced energy bandgap reduction of a perovskite by spin-orbit coupling via a low strength magnet. *J. Mater. Chem. C* **2020**, *8*, 4164–4168. [CrossRef]
7. Jeon, N.J.; Noh, J.H.; Yang, W.S.; Kim, Y.C.; Ryu, S.; Seo, J.; Seok, S.I. Compositional engineering of perovskite materials for high-performance solar cells. *Nature* **2015**, *517*, 476–480. [CrossRef]
8. Huang, Y.; Sun, Q.D.; Xu, W.; He, Y.; Yin, W.J. Halide perovskite materials for solar cells: A theoretical review. *Wuli Huaxue Xuebao/Acta Phys.Chim. Sin.* **2017**, *33*, 1730–1751.
9. Xu, A.F.; Wang, R.T.; Yang, L.W.; Liu, N.; Chen, Q.; LaPierre, R.; Isik Goktas, N.; Xu, G. Pyrrolidinium containing perovskites with thermal stability and water resistance for photovoltaics. *J. Mater. Chem. C* **2019**, *7*, 11104–11108. [CrossRef]
10. Park, B.-W.; Seok, S.I. Intrinsic Instability of Inorganic–Organic Hybrid Halide Perovskite Materials. *Adv. Mater.* **2019**, *31*, 1805337. [CrossRef]
11. Liu, N.; Du, Q.; Yin, G.; Liu, P.; Li, L.; Xie, H.; Zhu, C.; Li, Y.; Zhou, H.; Zhang, W.B.; et al. Extremely low trap-state energy level perovskite solar cells passivated using NH_2-POSS with improved efficiency and stability. *J. Mater. Chem. A* **2018**, *6*, 6806–6814. [CrossRef]
12. Liu, Z.; Sofia, S.E.; Laine, H.S.; Woodhouse, M.; Wieghold, S.; Peters, I.M.; Buonassisi, T. Revisiting thin silicon for photovoltaics: A technoeconomic perspective. *Energy Environ. Sci.* **2020**, *13*, 12–23. [CrossRef]
13. Tai, E.G.; Wang, R.T.; Chen, J.Y.; Xu, G. A water-stable organic-inorganic hybrid perovskite for solar cells by inorganic passivation. *Crystals* **2019**, *9*, 83. [CrossRef]
14. Zhou, H.; Chen, Q.; Li, G.; Luo, S.; Song, T.B.; Duan, H.S.; Hong, Z.; You, J.; Liu, Y.; Yang, Y. Interface engineering of highly efficient perovskite solar cells. *Science* **2014**, *345*, 542–546. [CrossRef] [PubMed]
15. Grancini, G.; Roldán-Carmona, C.; Zimmermann, I.; Mosconi, E.; Lee, X.; Martineau, D.; Narbey, S.; Oswald, F.; De Angelis, F.; Graetzel, M.; et al. One-Year stable perovskite solar cells by 2D/3D interface engineering. *Nat. Commun.* **2017**, *8*, 1–8. [CrossRef] [PubMed]
16. Wang, R.T.; Tai, E.G.; Chen, J.Y.; Xu, G.; LaPierre, R.; Goktas, N.I.; Hu, N. A $KMnF_3$ perovskite structure with improved stability, low bandgap and high transport properties. *Ceram. Int.* **2019**, *45*, 64–68. [CrossRef]
17. Pham, N.D.; Zhang, C.; Tiong, V.T.; Zhang, S.; Will, G.; Bou, A.; Bisquert, J.; Shaw, P.E.; Du, A.; Wilson, G.J.; et al. Tailoring Crystal Structure of $FA_{0.83}Cs_{0.17}PbI_3$ Perovskite Through Guanidinium Doping for Enhanced Performance and Tunable Hysteresis of Planar Perovskite Solar Cells. *Adv. Funct. Mater.* **2019**, *29*, 1806479. [CrossRef]

18. Wang, R.T.; Xu, A.F.; Chen, J.Y.; Yang, L.W.; Xu, G.; Jarvis, V.; Britten, J.F. Reversing Organic-Inorganic Hybrid Perovskite Degradation in Water via pH and Hydrogen Bonds. *J. Phys. Chem. Lett.* **2019**, *10*, 7245–7250. [CrossRef]
19. Eperon, G.E.; Stranks, S.D.; Menelaou, C.; Johnston, M.B.; Herz, L.M.; Snaith, H.J. Formamidinium lead trihalide: A broadly tunable perovskite for efficient planar heterojunction solar cells. *Energy Environ. Sci.* **2014**, *7*, 982–988. [CrossRef]
20. Chen, T.; Foley, B.J.; Park, C.; Brown, C.M.; Harriger, L.W.; Lee, J.; Ruff, J.; Yoon, M.; Choi, J.J.; Lee, S.H. Entropy-driven structural transition and kinetic trapping in formamidinium lead iodide perovskite. *Sci. Adv.* **2016**, *2*, e1601650. [CrossRef]
21. Eperon, G.E.; Paternò, G.M.; Sutton, R.J.; Zampetti, A.; Haghighirad, A.A.; Cacialli, F.; Snaith, H.J. Inorganic caesium lead iodide perovskite solar cells. *J. Mater. Chem. A* **2015**, *3*, 19688–19695. [CrossRef]
22. Steele, J.A.; Jin, H.; Dovgaliuk, I.; Berger, R.F.; Braeckevelt, T.; Yuan, H.; Martin, C.; Solano, E.; Lejaeghere, K.; Rogge, S.M.J.; et al. Thermal unequilibrium of strained black $CsPbI_3$ thin films. *Science* **2019**, *365*, 679–684. [CrossRef] [PubMed]
23. Pering, S.R.; Deng, W.; Troughton, J.R.; Kubiak, P.S.; Ghosh, D.; Niemann, R.G.; Brivio, F.; Jeffrey, F.E.; Walker, A.B.; Islam, M.S.; et al. Azetidinium lead iodide for perovskite solar cells. *J. Mater. Chem. A* **2017**, *5*, 20658–20665. [CrossRef]
24. Zheng, C.; Rubel, O. Aziridinium Lead Iodide: A Stable, Low-Band-Gap Hybrid Halide Perovskite for Photovoltaics. *J. Phys. Chem. Lett.* **2018**, *9*, 874–880. [CrossRef] [PubMed]
25. Xu, A.F.; Wang, R.T.; Yang, L.W.; Jarvis, V.; Britten, J.F.; Xu, G. Pyrrolidinium lead iodide from crystallography: A new perovskite with low bandgap and good water resistance. *Chem. Commun.* **2019**, *55*, 3251–3253. [CrossRef]
26. Liu, D.; Gangishetty, M.K.; Kelly, T.L. Effect of $CH_3NH_3PbI_3$ thickness on device efficiency in planar heterojunction perovskite solar cells. *J. Mater. Chem. A* **2014**, *2*, 19873–19881. [CrossRef]
27. Levchuk, I.; Herre, P.; Brandl, M.; Osvet, A.; Hock, R.; Peukert, W.; Schweizer, P.; Spiecker, E.; Batentschuk, M.; Brabec, C.J. Ligand-assisted thickness tailoring of highly luminescent colloidal $CH_3NH_3PbX_3$ (X = Br and I) perovskite nanoplatelets. *Chem. Commun.* **2017**, *53*, 244–247. [CrossRef]
28. Hintermayr, V.A.; Richter, A.F.; Ehrat, F.; Döblinger, M.; Vanderlinden, W.; Sichert, J.A.; Tong, Y.; Polavarapu, L.; Feldmann, J.; Urban, A.S. Tuning the Optical Properties of Perovskite Nanoplatelets through Composition and Thickness by Ligand-Assisted Exfoliation. *Adv. Mater.* **2016**, *28*, 9478–9485. [CrossRef]
29. Yuan, Z.; Zhou, C.; Tian, Y.; Shu, Y.; Messier, J.; Wang, J.C.; Van De Burgt, L.J.; Kountouriotis, K.; Xin, Y.; Holt, E.; et al. One-dimensional organic lead halide perovskites with efficient bluish white-light emission. *Nat. Commun.* **2017**, *8*, 1–7. [CrossRef]
30. Yang, M.; Zhang, T.; Schulz, P.; Li, Z.; Li, G.; Kim, D.H.; Guo, N.; Berry, J.J.; Zhu, K.; Zhao, Y. Facile fabrication of large-grain $CH_3NH_3PbI_{3-x}$ Brx films for high-efficiency solar cells via CH_3NH_3 Br-selective Ostwald ripening. *Nat. Commun.* **2016**, *7*, 12305. [CrossRef]
31. Yun, J.S.; Kim, J.; Young, T.; Patterson, R.J.; Kim, D.; Seidel, J.; Lim, S.; Green, M.A.; Huang, S.; Ho-Baillie, A. Humidity-Induced Degradation via Grain Boundaries of $HC(NH_2)_2PbI_3$ Planar Perovskite Solar Cells. *Adv. Funct. Mater.* **2018**, *28*, 1705363. [CrossRef]
32. Yang, J.; Siempelkamp, B.D.; Liu, D.; Kelly, T.L. Investigation of CH_3NH_3 PbI_3degradation rates and mechanisms in controlled humidity environments using in situ techniques. *ACS Nano* **2015**, *9*, 1955–1963. [CrossRef] [PubMed]
33. Chen, Q.; Zhou, H.; Song, T.B.; Luo, S.; Hong, Z.; Duan, H.S.; Dou, L.; Liu, Y.; Yang, Y. Controllable self-induced passivation of hybrid lead iodide perovskites toward high performance solar cells. *Nano Lett.* **2014**, *14*, 4158–4163. [CrossRef] [PubMed]
34. Conings, B.; Drijkoningen, J.; Gauquelin, N.; Babayigit, A.; D'Haen, J.; D'Olieslaeger, L.; Ethirajan, A.; Verbeeck, J.; Manca, J.; Mosconi, E.; et al. Intrinsic Thermal Instability of Methylammonium Lead Trihalide Perovskite. *Adv. Energy Mater.* **2015**, *5*, 1500477. [CrossRef]
35. Wu, Z.; Liu, Z.; Hu, Z.; Hawash, Z.; Qiu, L.; Jiang, Y.; Ono, L.K.; Qi, Y. Highly Efficient and Stable Perovskite Solar Cells via Modification of Energy Levels at the Perovskite/Carbon Electrode Interface. *Adv. Mater.* **2019**, *31*, 1804284. [CrossRef]